Mode Specificity Study in Unimolecular Dissociation of Nonrotating H_2O, DHO, and MuHO Molecules

J. L. Llanio-Trujillo, J. M. C. Marques, and A. J. C. Varandas*

Departamento de Química, Universidade de Coimbra, P-3049 Coimbra Codex, Portugal

Received: July 19, 1999; In Final Form: September 29, 1999

Classical trajectory calculations for the unimolecular dissociation of nonrotating H_2O, DHO, and MuHO are reported for different distributions of energy among the three vibrational normal modes. The calculations employ a realistic energy-switching potential energy surface for the electronic ground state of the water molecule. It is found that the unimolecular decay rates vary with the vibrational mode of the water molecule that is initially excited. Mode-selectivity has also been observed for DHO and MuHO, with the results being rationalized from inspection of the eigenvectors of the corresponding excited normal mode.

1. Introduction

The water molecule has long attracted the attention of dynamicists, kineticists, and spectroscopists. In particular, gas-phase reactions involving the H_2O molecule as an intermediate species have been for decades a subject of great interest from both the experimental[1−5] and theoretical[6,7] points of view. From the theoretical side, we refer to the recent dynamics study[7] on the $O(^1D) + H_2$ reaction, which plays an important role both in the atmospheric ozone chemistry and combustion processes. This study employed a realistic potential energy surface for water,[8] which was obtained from the energy-switching (ES) method by merging smoothly the local spectroscopic surface of Polyansky et al.[9] and the global many-body expansion (MBE) potential of Murrell et al.[10] (suitably adapted[8] to include the long-range dispersion forces). Since for linear H_2O geometries more than one electronic state can be involved, Varandas and co-workers[11,12] have extended the method to model the relevant manifold of electronic states. This implies the use of a multivalued (matrix form type) potential energy surface, which contrasts with the single-valued form used in ref 8.

In recent years, many theoretical studies have been devoted to the unimolecular dissociation of water:[13,14]

$$H_2O \rightarrow OH + H \qquad (1)$$

as well as to its intramolecular dynamics,[15−20] although most such studies have utilized simple model potential functions. Among them, we find some articles[18,19] that analyze the regular/chaotic behavior of the isotope-substituted DHO species. In those articles, the authors show that, for both H_2O and DHO, the classical dynamics is essentially regular at low levels of excitation, with the onset of chaos starting much earlier once the kinetic coupling is increased by a factor of 7 in the Hamiltonian model. In fact, using a realistic potential function,[21,22] Lawton and Child[16] have shown for H_2O that local- and normal-mode trajectories dominate at low energies, with the phase space being increasingly occupied by irregular trajectories for very high energies, mainly at the expenses of local motion; some regular normal-mode trajectories remain, even above the dissociation threshold in reaction 1. Moreover, Joseph et al.[13] performed simple model calculations of resonance states in H_2O and observed mode-selective decay that depends on the specific excitation of the stretching vibrations, that is, hyperspherical modes (stable) versus local modes (unstable). Such hyperspherical-type modes have also been found in the nonsymmetric DHO system but were absent in an equivalent model of MuHO, where the light muonium isotope replaced the deuterium atom.[14]

The quasiperiodic versus chaotic behavior of dynamical systems is a key question concerning the applicability of statistical methods to describe the corresponding unimolecular dissociation. Indeed, the well-known Rice−Ramsperger−Kassel−Marcus (RRKM) theory[23,24] is based on the assumptions that (a) all internal molecular states of energy above the threshold for dissociation are accessible, and (b) all such states have equal probabilities per unit of time of proceeding to products. These assumptions imply that the energized molecules will have a random lifetime distribution described by an exponential form, which is consistent with the fact that energized molecules may promptly decay or survive for many cycles of vibration. However, it is not infrequent to find examples of unimolecular processes that follow a non-RRKM type decay, such as in the isomerization of cyclopropane (see ref 25 and references therein). Usually, one distinguishes between apparent non-RRKM behavior and intrinsic non-RRKM behavior, the former arising from an initial specific state selection (e.g., by chemical activation), while the latter is due to bottlenecks in the energy transfer involving two or more vibrational degrees of freedom; this leads to a nonrandom lifetime distribution even if the vibrational states of the molecule are randomly prepared. In turn, it is common to classify the internal degrees of freedom into active if they exchange energy freely and adiabatic if they are associated to some quantity (e.g., the angular momentum) that is conserved during the reactive process; see ref 26, and references therein. Unimolecular dissociation rate constants are therefore expected to give an insight on the dynamics of the decaying complexes.

The aim of the present work is to investigate the influence of single isotope substitution in the dissociation dynamics of water. Note that the system loses its symmetry (C_{2v}), and the

* Corresponding author.

10.1021/jp992461g CCC: $18.00
Published on Web 11/19/1999

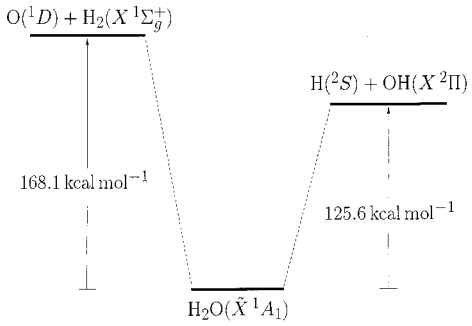

Figure 1. Schematic diagram of the main energetic features of the single-valued ES potential energy surface for the water molecule.

two bonds become nonequivalent, with possible implications on the dissociation dynamics. Since, for multidimensional systems described by intricate potential energy surfaces, it is not easy to achieve a priori an understanding of the involved phase space dynamics, a study of the unimolecular decay rates such as the present one becomes a simpler tool toward that goal; see, for example, ref 26. The paper is organized as follows. Section 2 presents the computational procedure, including a description of the most relevant features of the potential energy surface (Subsection 2.1), the trajectory methodology (Subsection 2.2), and the kinetic models (Subsection 2.3). The results are discussed in Section 3, while the conclusions are in Section 4.

2. Computational Method

2.1 Potential Energy Surface. All calculations employed the single-valued potential energy surface for the water molecule that was obtained from the energy-switching[8] (ES) method. Specifically, it was obtained by merging smoothly a local surface[9] that accurately reproduces the spectroscopy of the water molecule with a global one[27] that properly describes its dissociation limits. This surface, due to Murrell and Carter, has been suitably modified[8] to include long-range dispersion forces. In particular, the two-body extended-Rydberg curves originally used in the MBE form to describe the electronic ground states of H_2 and OH were replaced with more accurate extended Hartree-Fock approximate correlation energy (EHFACE2U)[28,29] functions which show the proper asymptotic behavior both at $R \rightarrow 0$ and $R \rightarrow \infty$.

Since the main features of the ES potential energy surface for the water molecule have been described in detail elsewhere,[8] we just present here the energetics relevant for the present work. This is illustrated in Figure 1, which shows the energy separation between the minimum of the potential energy surface (associated with the equilibrium C_{2v} H_2O structure) and the dissociative channels $O(^1D) + H_2(X^1\Sigma_g^+)$ and H + OH. Of course, in the case of DHO (MuHO), the dissociation leading to D + OH (Mu + OH) and H + OD (H + OMu) has classically the same energy threshold as H + OH, that is 125.6 kcal mol^{-1}. In contrast, the upper dissociation channel leads to $O(^1D)$ + H_2, $O(^1D)$ + HD, and $O(^1D)$ + HMu, respectively, for H_2O, DHO, and MuHO. This dissociation channel arises, in all cases, for the same classical energy threshold of 168.1 kcal mol^{-1} above the minimum of the potential energy surface for the water molecule.

2.2 Trajectory Calculations. All trajectory calculations employed an extensively adapted version of the MERCURY code,[30] with an optimum integration time-step of 2.5×10^{-5} ps. For most initial conditions, it was judged sufficient to run 500 trajectories. Some exceptions are indicated in Table 1; for these, 5000 trajectories were run to clarify the decaying behavior of the corresponding triatomic complexes. The initial vibrational excitation energies cover the range $131.35 \leq E_v/\text{kcal mol}^{-1} \leq 147.62$, and hence the channel leading to O + HX (X stands for H, D or Mu) always remains closed; see Figure 1. Thus, the only formed products are H + OH for H_2O; H + OD and D + OH for DHO; and Mu + OH and H + OMu for MuHO.

TABLE 1: Summary of Trajectory Calculations for the Unimolecular Dissociation of H_2O, DHO, and MuHO Systems

	normal-mode energies/kcal mol^{-1}			products				
system	E_1	E_2	E_3	N_{OH}	N_{OX}	$f_{\langle E_v \rangle}$	$f_{\langle E_r \rangle}$	$f_{\langle E_{tr} \rangle}$
H_2O	120.23	5.48	5.64	*a*	*a*	0.46	0.16	0.38
	2.36	126.13	5.64	*a*	*a*	0.48	0.14	0.38
	2.36	5.48	129.78	*a*	*a*	0.53	0.13	0.34
	b	*b*	*b*	*a*	*a*	0.45	0.15	0.40
	130.23	5.48	5.64	*a*	*a*	0.46	0.17	0.37
	2.36	136.13	5.64	*a*	*a*	0.57	0.11	0.32
	2.36	5.48	139.78	*a*	*a*	0.63	0.08	0.29
	c	*c*	*c*	*a*	*a*	0.47	0.14	0.39
DHO	120.23	5.48	5.64	155	345	0.43 (0.38)	0.16 (0.19)	0.41 (0.43)
	2.36	126.13	5.64	439	61	0.51 (0.48)	0.06 (0.18)	0.43 (0.34)
	2.36	5.48	129.78	18	482	0.44 (0.45)	0.16 (0.06)	0.40 (0.49)
	b	*b*	*b*	202	298	0.43 (0.42)	0.15 (0.15)	0.42 (0.43)
	130.23	5.48	5.64	130	370	0.41 (0.41)	0.15 (0.19)	0.44 (0.40)
	2.36	136.13	5.64	480	20	0.33 (0.53)	0.03 (0.09)	0.64 (0.38)
	2.36	5.48	139.78	99[d]	4901[d]	0.47 (0.30)	0.13 (0.04)	0.40 (0.66)
	c	*c*	*c*	216	284	0.45 (0.46)	0.14 (0.16)	0.41 (0.38)
MuHO	120.23	5.48	5.64	371	129	0.54 (0.45)	0.16 (0.19)	0.30 (0.36)
	2.36	126.13	5.64	857[d]	4143[d]	0.55 (0.30)	0.16 (0.27)	0.29 (0.43)
	2.36	5.48	129.78	485	15	0.41 (0.52)	0.04 (0.19)	0.55 (0.29)
	b	*b*	*b*	333	167	0.54 (0.49)	0.16 (0.17)	0.30 (0.34)
	130.23	5.48	5.64	408	92	0.52 (0.45)	0.17 (0.21)	0.31 (0.34)
	2.36	136.13	5.64	34	466	0.62 (0.32)	0.14 (0.05)	0.24 (0.63)
	2.36	5.48	139.78	4940[d]	60[d]	0.28 (0.37)	0.02 (0.23)	0.70 (0.40)
	c	*c*	*c*	338	162	0.55 (0.46)	0.14 (0.16)	0.30 (0.38)

[a] For H_2O, all trajectories dissociate to form OH products. [b] The microcanonical distribution was used to attribute randomly a total of 131.35 kcal mol^{-1} along the three vibrational modes. [c] The microcanonical distribution was used to attribute randomly a total of 141.35 kcal mol^{-1} along the three vibrational modes. [d] The total number of trajectories is 5000.

TABLE 2: Kinetic Parameters Obtained Using Models of Subsection 2.3 for Unimolecular Dissociation of the Title Systems[a]

	normal-mode energies/kcal mol^{-1}			kinetic parameters					
system	E_1	E_2	E_3	f_A^0	f_A^0	k_1/ps^{-1}	k_2/ps^{-1}	k_3/ps^{-1}	k_4/ps^{-1}
H_2O[b]	120.23	5.48	5.64						0.73
	2.36	126.13	5.64						1.31
	2.36	5.48	129.78						1.66
	b	*b*	*b*						0.86
	130.23	5.48	5.64						2.06
	2.36	136.13	5.64						2.64
	2.36	5.48	139.78						3.29
	c	*c*	*c*						2.50
DHO	120.23	5.48	5.64						0.67 (0.81)
	2.36	126.13	5.64	0.14	0.12	2.10	0.84	4.29	36.65 (0.98)
	2.36	5.48	129.78	(0.11)	(0.14)	(2.58)	(0.0[e])	(115.04)	1.63 (88.07)
	b	*b*	*b*						0.80 (0.79)
	130.23	5.48	5.64						2.19 (2.14)
	2.36	136.13	5.64	0.01	0.07	5.04	0.0[e]	14.78	95.04 (2.79)
	2.36	5.48	139.78	(0.04)	(0.07)	(7.49)	(3.06)	(13.21)	2.63 (131.70)
	c	*c*	*c*						2.02 (2.40)
MuHO	120.23	5.48	5.64						0.71 (0.57)
	2.36	126.13	5.64	(0.15)	(0.20)	(2.22)	(0.88)	(4.57)	0.72 (47.21)
	2.36	5.48	129.78	0.07	0.04	2.02	0.04	11.29	288.39 (1.22)
	b	*b*	*b*						0.64 (0.61)
	130.23	5.48	5.64						2.39 (1.92)
	2.36	136.13	5.64	(0.04)	(0.10)	(2.57)	(0.0[e])	(2.87)	2.00 (125.24)
	2.36	5.48	139.78	0.03	0.03	6.00	0.10	7.50	589.94 (2.43)
	c	*c*	*c*						2.13 (2.00)

[a] All values in parenthesis refer to the dissociation rate coefficients and corresponding initial fractions of A-type and B-type complexes for OX (X ≡ D or Mu) formation. Blank entries refer to RRKM behavior and imply that the corresponding coefficients are meaningless. [b] For H_2O, all initial conditions lead to RRKM behavior and $f_C^0 = 1$, since $f_A^0 = f_B^0 = 0$. [c] The microcanonical distribution was used to attribute randomly a total of 131.35 kcal mol^{-1} among the three vibrational modes. [d] The microcanonical distribution was used to attribute randomly a total of 141.35 kcal mol^{-1} among the three vibrational modes. [e] k_2 was fixed to zero during the fitting procedure.

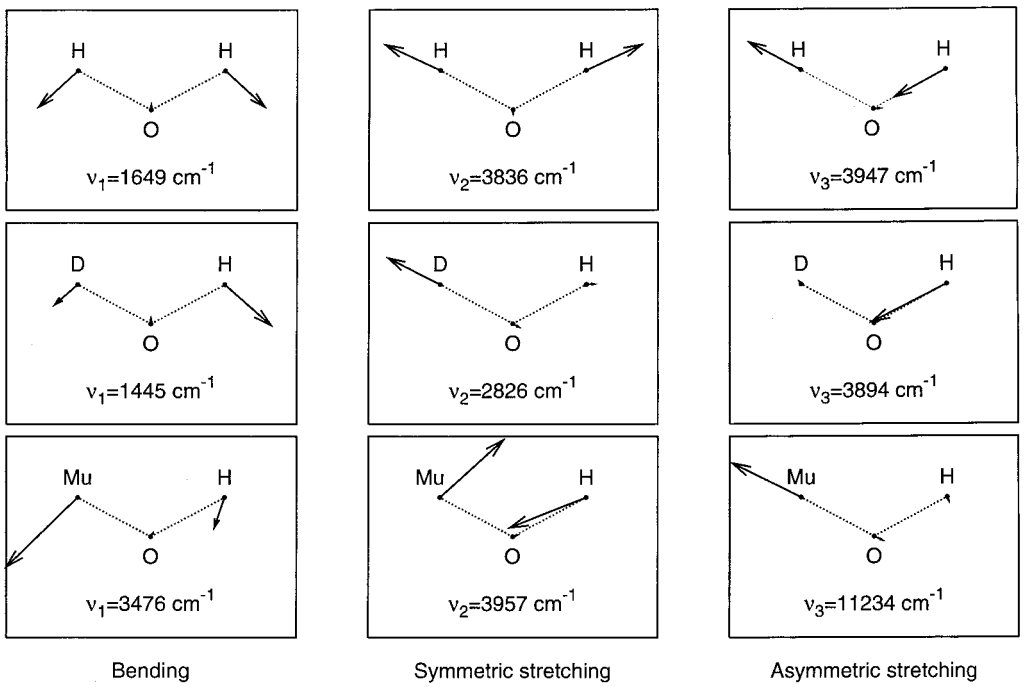

Figure 2. Schematic representation of the three normal modes of vibration for H_2O. The fundamental frequencies obtained for bending, symmetric stretching, and asymmetric stretching are also given in cm^{-1}. The corresponding data for DHO and MuHO are also given; see the text.

Table 1 and Table 2 summarize the trajectory results; for H + OD and H + OMu, they are given in parenthesis.

We initiated the present study with a normal-mode analysis of the title systems. A schematic presentation of the corresponding eigenvectors is given in Figure 2, which also indicates the associated normal-mode frequencies. Clearly, there are three possibilities for initially exciting the triatomic system, depending on which normal mode one considers: bending (ν_1), symmetric stretching (ν_2) or asymmetric stretching (ν_3). Note that this kind of nomenclature is appropriate only for H_2O, although we will also use it for the isotopically substituted water molecules. Thus, in DHO and MuHO, such modes are the ones that result when the mass of H is continuously varied until it equals that of D or Mu in the above order. All such mode-specific excitations were considered in the present work. Moreover, we considered an initial preparation of the system via a microcanonical distribution of the vibrational energy. In addition, for all four types of initial preparation, two energy levels of excitation were considered:

one corresponds to a total energy of just a few kcal mol^{-1} above the dissociation threshold; the other has an extra 10 kcal mol^{-1} (see Table 1 and Table 2).

2.3 Kinetic Models. In previous work,[31,32] we described non-RRKM behavior by assuming the following two-step mechanism:

$$\mathrm{B} \xrightarrow{k_3} \mathrm{C} \xrightarrow{k_4} \text{products} \tag{2}$$

where B (C) stands for a molecular species not coupled (strongly coupled) with the reaction path, and the rate coefficients (denoted k_3 and k_4 to be consistent with the notation used in the present work) follow the relation $k_3 < k_4$ or $k_3 \ll k_4$. The calculated fraction of nondissociated species at each moment was then fitted to the form[31]

$$f(t) = f_\mathrm{B} + f_\mathrm{C} = \left(f_\mathrm{C}^0 - \frac{k_3 f_\mathrm{B}^0}{k_4 - k_3}\right)\exp(-k_4 t) + \left(\frac{k_3 f_\mathrm{B}^0}{k_4 - k_3} + f_\mathrm{B}^0\right)\exp(-k_3 t) \tag{3}$$

where f_B and f_C are the fractions of B and C at time t, and f_B^0 and f_C^0 are the corresponding values for $t = 0$. Note that, if $f_\mathrm{B}^0 = 0$, eq 3 reduces to

$$f(t) = f_C^0 \exp(-k_4 t) \tag{4}$$

and hence the logarithm of the decay rate is a straight line, as expected from RRKM theory.

Since the above two-step mechanism may be too simplistic to adequately describe the decaying behavior of the title systems, especially for certain initial conditions, we also examined a more elaborate scheme that contains the model in eq 2 as a particular case. Thus, three types of energized species are postulated: complexes with a great content of energy associated with the reaction path that immediately decompose to yield products (C-type); complexes with an energy essentially associated to coordinates other than the reaction path but coupled with it (B-type); and complexes with most of the energetic content in the coordinate less coupled to the reaction (A-type). Such a model may be represented by

$$\mathrm{A} \underset{k_2}{\overset{k_1}{\rightleftharpoons}} \mathrm{B} \xrightarrow{k_3} \mathrm{C} \xrightarrow{k_4} \text{products} \tag{5}$$

It should be noted that in this model it is not possible to form B-type species from C-type ones due to the prompt dissociation of the latter. In contrast, since there is a strong coupling in the B-type complexes, these may form or reform A-type ones, with such a possibility depending on the initial amount of those complexes and their corresponding dissociative rates. The scheme in eq 5 leads to a set of three differential equations whose analytical solution is

$$f(t) = f_\mathrm{A} + f_\mathrm{B} + f_\mathrm{C} = \left(f_\mathrm{A}^0 - \frac{k_3 f_\mathrm{B}^0}{k_1 - k_2} + \frac{k_1 f_\mathrm{A}^0}{k_{23} - k_1}\right)\exp(-k_1 t) + \frac{k_2 f_\mathrm{B}^0}{k_1 - k_2}\exp(-k_2 t) + \left(f_\mathrm{B}^0 - \frac{k_1 f_\mathrm{A}^0}{k_{23} - k_1}\right)\exp(-k_{23} t) + \frac{k_3 f_\mathrm{B}^0}{k_4 - k_3}\exp(-k_3 t) + \left(f^0{}_\mathrm{C} - \frac{k_3 f_\mathrm{B}^0}{k_4 - k_3}\right)\exp(-k_4 t) \tag{6}$$

where $k_{23} = k_2 + k_3$ and f_A^0, f_B^0, and f_C^0 are the initial fractions of complexes A, B, and C, respectively. As before, since the requirement $f_\mathrm{A}^0 + f_\mathrm{B}^0 + f_\mathrm{C}^0 = 1$ must be fulfilled, we have six fitting parameters, namely, f_A^0, f_B^0, k_1, k_2, k_3, and k_4. Note also that eq 3 may be obtained from eq 6 when $f_\mathrm{A}^0 = 0$ and $k_2 = 0$. Of course, both conditions are independent from each other, and the latter is expected to arise when $k_3 \gg k_1$, while the former is supposed to be related to the specific preparation of the dissociative complexes.

The model in eq 5 is similar to one proposed by Davis,[33] in which a strong bottleneck in the phase space was considered. We show here that such a model is also viable in rationalizing intramolecular vibrational energy redistribution followed by dissociation whenever the energy is not randomly distributed among the various degrees of freedom.

3. Results and Discussion

The decaying behavior in the unimolecular dissociation $H_2O \rightarrow OH + H$ is shown in Figure 3 for different kinds of vibrational mode excitation; the corresponding numerical values are given in Table 1 and Table 2. It is clear from Figure 3 that all the unimolecular rate decays follow a straight line behavior described by the logarithm of eq 4. However, the unimolecular rate coefficients are bigger in the case of stretching excitation (both symmetric and asymmetric) than for the case of an excess of energy in the bending mode; see also Table 2. This is not surprising, since the stretching motion is expected to be more associated with the reaction path than the bending motion (see Figure 2). Additionally, it is seen from Table 1 that the fraction of mean vibrational energy of the forming OH products ($f_{\langle E_\mathrm{v}\rangle}$) is somewhat larger in the case of the stretching excitations at the expense of the corresponding fractions of the mean translational ($f_{\langle E_\mathrm{tr}\rangle}$) and rotational ($f_{\langle E_\mathrm{r}\rangle}$) energies, in particular when the higher level of initial vibrational excitation is considered; this indicates that such excitations do not allow a total randomization of energy among the various degrees of freedom. Conversely, the fraction of mean rotational energy in the products ($f_{\langle E_\mathrm{r}\rangle}$) is slightly higher for the initial bending excitation than for the stretching ones, which is again not unexpected, since the bending eigenvectors are essentially orthogonal to the O−H bonds.

Another interesting finding is that the microcanonical initial preparation leads to a decay rate close to, yet bigger than, the bending excitation. Indeed, since the molecule is uniformly excited whenever it is prepared through a microcanonical sampling, the single-mode smallest rate (i.e., the bending) will control the microcanonical rate. We should also note that the fractions of the mean values of vibrational, rotational, and translational energy in the products are always similar for both microcanonical preparation and bending excitation. For both cases, the values of $f_{\langle E_\mathrm{v}\rangle}$, $f_{\langle E_\mathrm{r}\rangle}$, and $f_{\langle E_\mathrm{tr}\rangle}$ keep approximately the same values in going to the higher level of initial excitation considered in the present work. This clearly indicates that, in contrast with the initial stretching excitations, the microcanonical sampling and bending excitation lead to a considerable amount of energy randomization among all degrees of freedom. In summary, both symmetric and asymmetric stretching modes are more associated with the reaction path than the bending mode, and hence lead to larger rate coefficients and a smaller randomization of energy. However, due to coupling of the three normal modes (although in different extents) with the reaction path, there are no bottlenecks in phase space that can prevent trajectories from dissociating at the same rate, as it is clear from the straight lines shown in Figure 3 for each particular case.

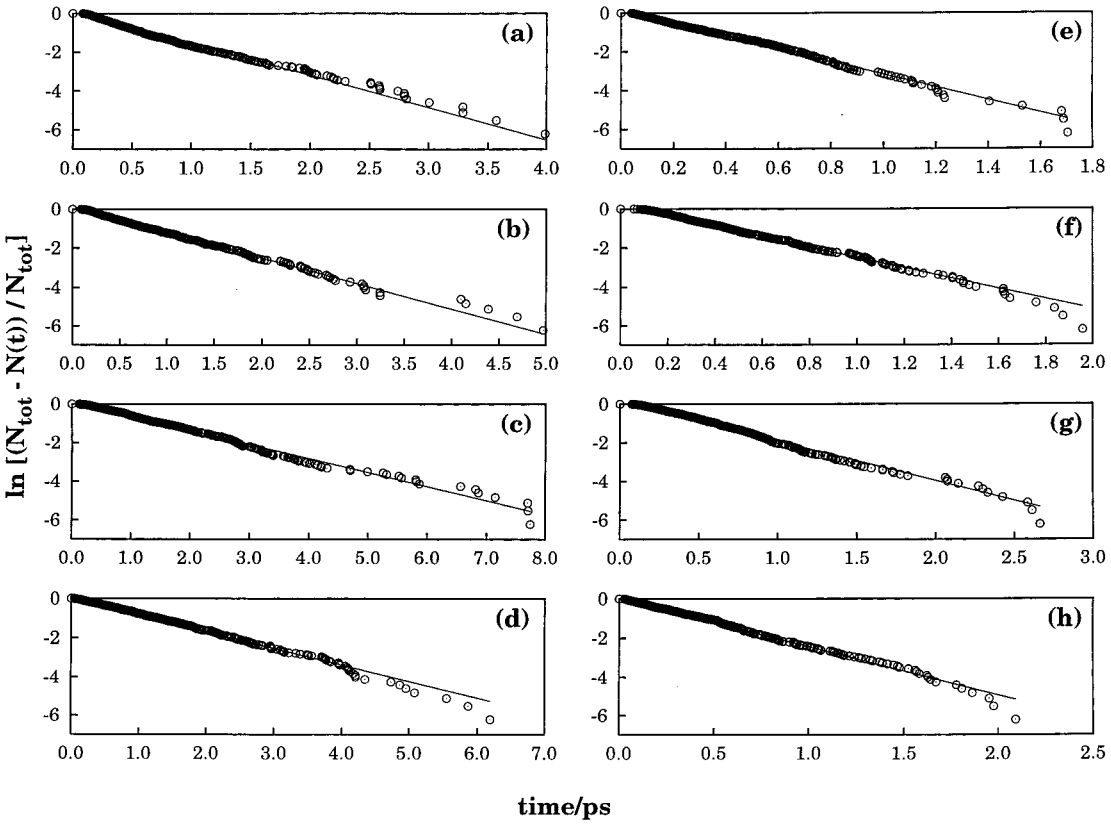

Figure 3. Logarithm of the decay rates for H_2O as a function of time. Lower level of initial vibrational excitation: (a) bending; (b) symmetric stretching; (c) asymmetric stretching; (d) microcanonical. Higher level of initial vibrational excitation: (e) bending; (f) symmetric stretching; (g) asymmetric stretching; (h) microcanonical. See also Table 2.

Furthermore, the decay rates present an obvious increase as the energy content increases in the excited modes.

The results for H_2O reported in the present work can be used as a comparison basis for DHO and MuHO. Note that although the dynamics of these systems occurs on the same potential surface, DHO and MuHO are no longer symmetric. As a result, H_2O dissociation always leads to formation of OH while two different reactive channels appear for the other systems: D + OH and H + OD for DHO; Mu + OH and H + OMu for MuHO. Table 1 indicates that formation of OD is favored for initial bending excitation and asymmetric stretching, as might have been anticipated from a visual analysis of the corresponding eigenvectors in Figure 2. Note that, due to mass differences, the hydrogen atom executes a faster motion during the bending of DHO. Since for the asymmetric stretching case, the H motion is more strongly coupled to the reaction path in the sense of favoring OD + H products, the ratio N_{OD}/N_{OH} increases even more dramatically. Conversely, the symmetric stretching involves mainly the stretch of the O−D bond, and hence OH formation is clearly favored. This mode selectivity in products formation is enhanced when the level of energy excitation is increased. Due to the fact that two of the three normal modes lead mainly to formation of OD, it is expected that, for the microcanonical preparation, the H + OD dissociative channel is still slightly preferred. The MuHO system also shows mode selectivity, but due to Mu having a much smaller mass than H, the effect now arises in the opposite sense: the bending, asymmetric stretching, and microcanonical preparations favor OH formation, while the symmetric excitation leads preferentially to OMu (see Table 1).

Figure 4 shows the decay rates for the dissociation of DHO to form OH + D or OD + H products. Microcanonical preparation leads to a straight-line behavior in Figure 4d and Figure 4h both for OH and OD formation, while the corresponding values for the decay rate coefficients (k_4) are given in Table 2. Note that the values of k_4 increase, in this case, with increasing energization; for the same energy content, they have the same order of magnitude as in H_2O microcanonical dissociation. Once more, similar results are obtained for bending excitation. This means that the bending mode allows an easy randomization of the vibrational energy among all degrees of freedom. In fact, the fractions of the mean values of vibrational ($f_{\langle E_v \rangle}$), rotational ($f_{\langle E_r \rangle}$), and translational ($f_{\langle E_{tr} \rangle}$) energy show similar values for both D + OH and H + OD products (although favoring somewhat more translation than those for H_2O dissociation) while presenting only a small comparative oscillation between the two levels of excitation. In contrast, stretching excitations give rather different values for $f_{\langle E_r \rangle}$ in the two arising channels: the symmetric stretch leads to values of 0.06 (0.18) and 0.03 (0.09) for OH (OD) at the lower and higher levels of excitation, respectively; the asymmetric stretch gives 0.16 (0.06) and 0.13 (0.04) in the same order. This clear tendency of $f_{\langle E_r \rangle}$ to decrease in both D + OH and H + OD channels as the stretching energization increases is not generally followed by a similar decrease in $f_{\langle E_v \rangle}$ and $f_{\langle E_{tr} \rangle}$, which show opposite variations due mainly to vibration−translation interchange. Since both symmetric and asymmetric stretching normal modes in DHO (Figure 2) are essentially localized in the O−D and O−H bonds, respectively, the increase of the energy content in those modes leads to prompt formation of the corresponding D + OH or H + OD products with larger values for $f_{\langle \mathbf{E_{tr}} \rangle}$. In turn, since the total energy must be constant, the associated values of $f_{\langle E_v \rangle}$ have to decrease with increasing energization. Such a pattern shows that the randomization of energy is more difficult whenever the DHO molecules are prepared with initial excitation in the stretching (both symmetric and asymmetric) normal modes. This

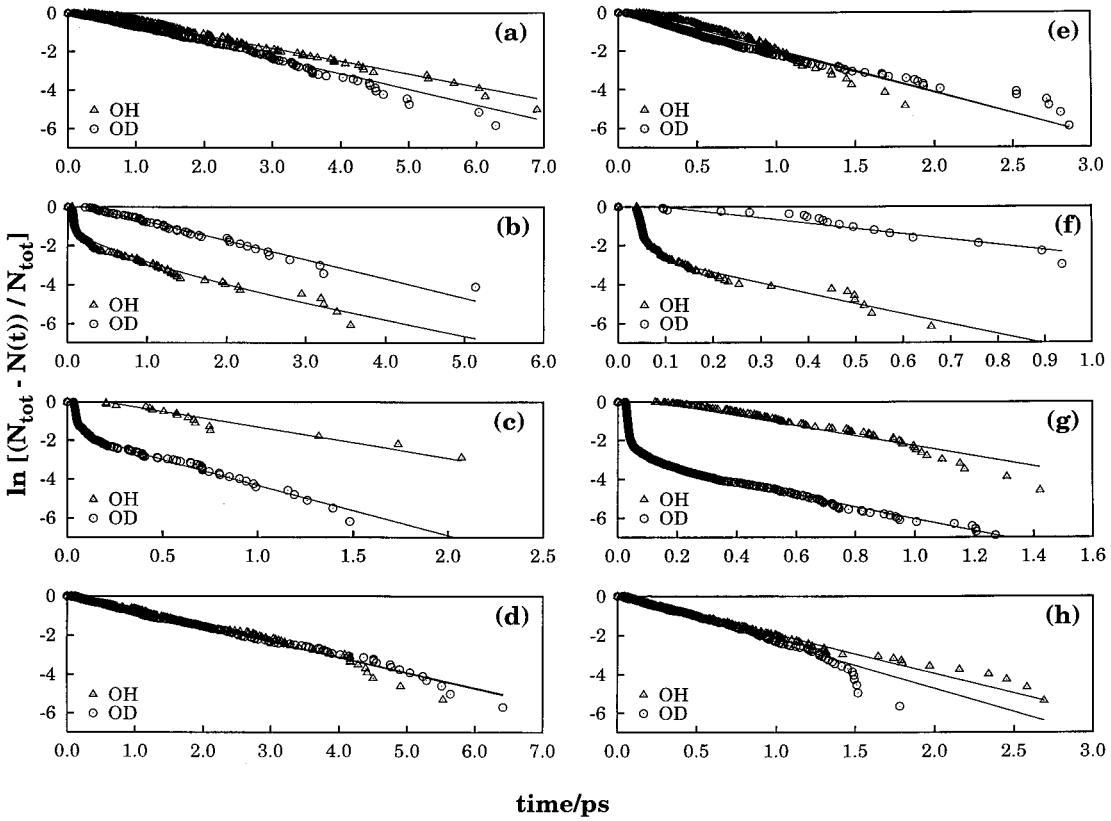

Figure 4. Logarithm of the decay rates for DHO as a function of time. Panels are as in Figure 3. The open circles correspond to H + OD formation while the open triangles are for D + OH. Note that the two fitted lines are nearly indistinguishable in the case of plots (d) and (e).

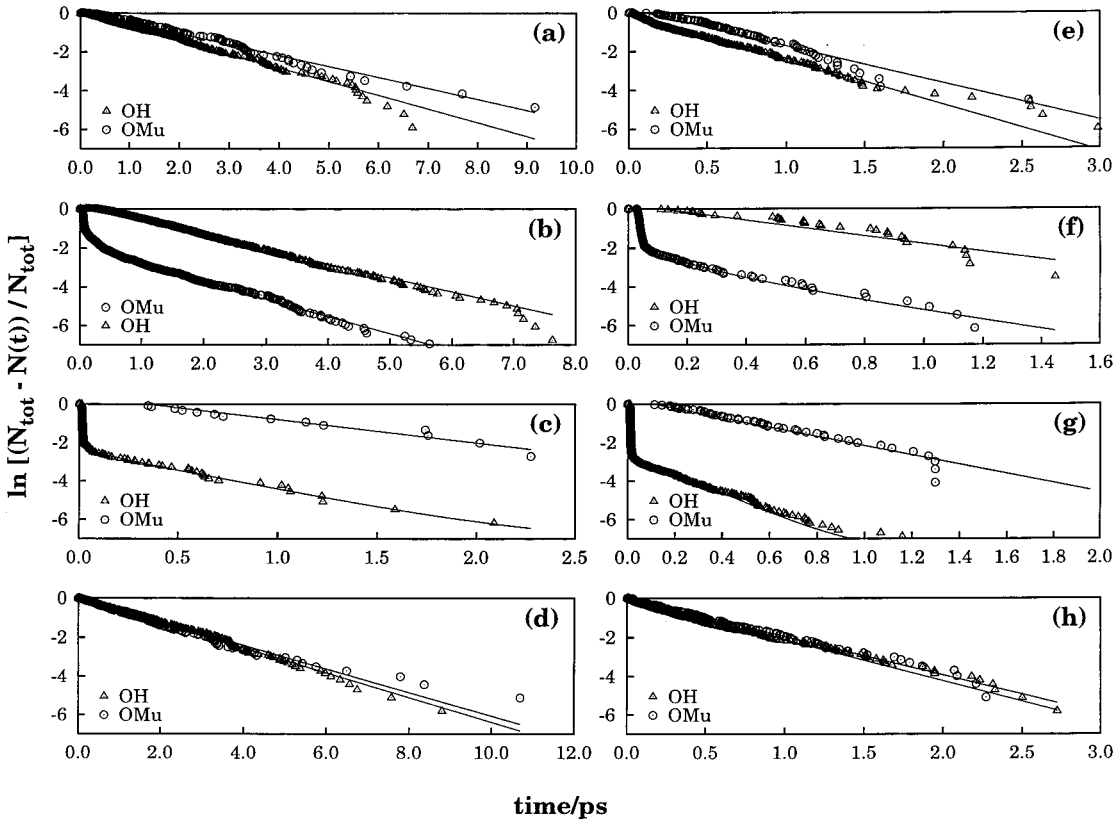

Figure 5. Logarithm of the decay rates for MuHO as a function of time. Panels are as in Figure 3. The open circles correspond to H + OMu formation while the open triangles are for Mu + OH.

difficulty even increases with the energy content due to the faster dissociation of most DHO complexes, which does not allow a proper randomization of energy.

Concerning the decay rate coefficients for the symmetric and asymmetric stretching excitations of DHO, we generally considered the kinetic model of eq 5, whose parameters were then

fitted using eq 6 and the numerical data obtained from the trajectory calculations. It is important to stress that k_2 may be fixed to zero whenever k_3 is, at least, about one order of magnitude larger than k_1. This procedure, together with a judicious weighting of the calculated points, has shown to be essential to reproduce the correct decaying behavior of the dissociating complexes, especially in the cases where f_A^0 and f_B^0 are too small in comparison with f_C^0. Also shown are the corresponding fitted curves: for the symmetric stretching in Figure 4(b) and Figure 4(f); for the asymmetric stretching excitation in Figure 4(c) and Figure 4(g). The numerical values of the kinetic parameters arising in all fits are given in Table 2. Note from this table that both symmetric and asymmetric vibrational mode excitations prepare most of the DHO complexes with a great amount of energy associated with the corresponding reaction coordinate (C-type), which leads to a prompt dissociation of such energized species. However, due to the coupling of the two bonds, a flux of energy may occur from O−D (O−H) to O−H (O−D) in the case of the symmetric (asymmetric) excitation, which may be associated with the appearance of species A and B in the suggested kinetic model. Note that, in contrast with H_2O, the attribution of vibrational energy to DHO (as well as MuHO) leads to a local-mode-type excitation in the case of the symmetric and asymmetric stretchings; this excitation is localized in the O−D or O−H bonds. Among the various complexes, we have already referred to those of type-C (prompt to dissociate); for the type-A and type-B complexes, one may speculate, based on simple IVR models,[34,35] that they arise from an aperiodic energy transfer caused by the simultaneous overlap of various nonlinear resonances that have to be taken into account for high energy excitations. The trajectories with a more complex dynamics, that is, those involving A-type and B-type species, may dissociate to form either H + OD (D + OH) or D + OH (H + OD) products, the corresponding rates of decay being essentially the same for the case of the symmetric (asymmetric) stretching excitation. Indeed, the dissociation of A-type and B-type complexes are controlled essentially by the smaller of k_1 and k_3, such a value being of the same order of magnitude as k_4 for the alternative formation of H + OD (D + OH) due to the initial symmetric (asymmetric) stretching excitation. Note also that, as the level of stretching excitation increases, the flux of energy is no longer viable, and hence f_A^0 and f_B^0 are expected to decrease; this is associated with a corresponding decrease in the fraction of trajectories which proceed via the alternative dissociation channel.

Finally, Figure 5 shows the decay rates for dissociation of MuHO into Mu + OH or H + OMu; for the corresponding numerical values, see Table 2. We conclude from Figure 5 that the dissociation behavior for MuHO shows a similar pattern as the DHO. Indeed, for each set of initial conditions, at least one of the two possible dissociative channels leads to a RRKM-type behavior while the other may show various decaying regimes, namely, for the stretching mode excitations. Also, for both DHO and MuHO systems, the symmetric stretching mode excitation leads to more A-type and B-type complexes than the asymmetric one, this difference being rather more significant in the case of MuHO. This may be attributed to the fact that O−H and O−X (X ≡ D or Mu) coordinates must be more coupled in the case of the symmetric mode excitation, perhaps due to some tendency of the lighter atom to move out of the bond axis, which is clearly seen in Figure 2 for the MuHO system. Note that the symmetric stretching and bending frequencies have similar values for MuHO in contrast to the cases of H_2O and HDO, in which the two stretchings are more similar to each other than to the bending mode. Moreover, it is important to note that, due to the larger difference of masses in the case of MuHO, the asymmetric stretching mode excitation provides a much more significant fraction of the dissociating complexes with a great amount of vibrational energy associated with the O−Mu bond (i.e., C-type complexes), so that the triatomic species promptly dissociates with few possibilities of exchanging energy among other degrees of freedom. In fact, the asymmetric mode excitation clearly presents larger values of k_4 for MuHO than for DHO, which may be explained by considering that a larger amount of energy is attributed to the breaking O−Mu bond than to the O−H one, due to the relative lightness of Mu atom.

4. Conclusions

We have carried out a classical trajectory study of the unimolecular dissociation of nonrotating H_2O, DHO, and MuHO systems for different initial vibrational normal-mode excitations. The calculations employed the realistic single-valued energy-switching potential energy surface for the ground electronic state of the water molecule. Since the flux of energy to the reaction coordinate is large enough in H_2O, a RRKM-type behavior was observed for all decay rates. Conversely, for DHO and MuHO, apparent non-RRKM behavior was observed when the stretching modes were excited, leading to RRKM behavior for the bending and microcanonical initial preparations. It has also been shown that DHO and MuHO present mode selectivity in the outcoming products, which has been attributed to the breakdown of the symmetry of the water molecule due to isotope substitution. Additionally, a three-step mechanism involving an interconversion between two (A and B) of the energized species was shown to describe well the apparent non-RRKM decaying behavior of DHO and MuHO. Such species are associated to different regions of the phase space of the triatomic system which correspond to different ways of localizing and transferring energy among the relevant modes.

Acknowledgment. One of us (J.L.L.T.) thanks the Ministerio de Ciencia Tecnologia y Medio Ambiente (Pinar del Rio, Cuba) for a leave of absence. The financial support from Fundação para a Ciência e Tecnologia, Portugal, under programme PRAXIS XXI is gratefully acknowledged.

References and Notes

(1) Young, R. A.; Black, G.; Slanger, T. G. *J. Chem. Phys.* **1968**, *49*, 4758.
(2) Heidner, R. F.; Husain, D. *Int. J. Chem. Kinet.* **1973**, *5*, 819.
(3) Stief, L. P.; Payne, W. A.; Klemm, R. B. *J. Chem. Phys.* **1975**, *62*, 4000.
(4) Davidson, J. A.; Sadowski, C. M.; Schiff, H. I.; Streit, G. E.; Howard, C. J.; Jennings, D. A.; Schmeltkopf, A. L. *J. Chem. Phys.* **1976**, *64*, 57.
(5) Atkinson, R.; Baulch, D. L.; Cox, R. A.; Hampson, R. F., Jr.; Kerr, J. A.; Troe, J. *J. Phys. Chem. Ref. Data* **1992**, *21*, 1125.
(6) Schinke, R.; Lester, W. A. *J. Chem. Phys.* **1980**, *72*, 3754.
(7) Varandas, A. J. C.; Voronin, A. I.; Riganelli, A.; Caridade, P. J. S. B. *Chem. Phys. Lett*. **1997**, *278*, 325.
(8) Varandas, A. J. C. *J. Chem. Phys*. **1996**, *105*, 3524.
(9) Polyansky, O. L.; Jensen, P.; Tennyson, J. *J. Chem. Phys*. **1994**, *101*, 7651.
(10) Murrell, J. N.; Carter, S.; Mills, I. M.; Guest, M. F. *Mol. Phys*. **1981**, *42*, 605.
(11) Varandas, A. J. C. *J. Chem. Phys*. **1997**, *107*, 867.
(12) Varandas, A. J. C.; Voronin, A. I.; Caridade, P. J. S. B. *J. Chem. Phys*. **1998**, *108*, 7623.
(13) Joseph, T.; Kruel, T.-M.; Manz, J.; Rexrodt, I. *Chem. Phys*. **1987**, *113*, 223.

(14) Hartke, B.; Manz, J.; Mathis, J. *J. Chem. Phys.* **1989**, *139*, 123.
(15) Møler, H. S.; Mortensen, O. S. *Chem. Phys. Lett*. **1979**, *66*, 539.
(16) Lawton, R. T.; Child, M. S. *Mol. Phys*. **1981**, *44*, 709.
(17) Sibert, E. L.; Reinhardt, W. P.; Hynes, J. T. *J. Chem. Phys*. **1982**, *77*, 3583.
(18) Skodje, R. T.; Borondo, F.; Reinhardt, W. P. *J. Chem. Phys*. **1985**, *82*, 4611.
(19) Skodje, R. T.; Borondo, F. J. *J. Chem. Phys.* **1986**, *85*, 2760.
(20) Fukui, K.; Cline, J. I.; Frederick, J. H. *J. Chem. Phys*. **1997**, *107*, 4551.
(21) Lawton, R. T.; Child, M. S. *Mol. Phys*. **1980**, *40*, 773.
(22) Sorbie, K. S.; Murrell, J. N. *Mol. Phys*. **1975**, *29*, 1387.
(23) Marcus, R. A. *J. Chem. Phys.* **1952**, *20*, 359.
(24) Marcus, R. A.; Rice, O. K. *J. Phys. Colloid Chem*. **1951**, *55*, 894.
(25) Hase, W. L. *Acc. Chem. Res*. **1998**, *31*, 659.
(26) Marques, J. M. C.; Varandas, A. J. C. *J. Phys. Chem*. **1997**, *101*, 5168.
(27) Murrell, J. N.; Carter, S. *J. Phys. Chem*. **1984**, *88*, 4887.
(28) Varandas, A. J. C.; Silva, J. D. *J. Chem. Soc., Faraday Trans.* **1992**, *88*, 941.
(29) Varandas, A. J. C.; Voronin, A. I. *Chem. Phys*. **1995**, *194*, 91.
(30) Hase, W. L. MERCURY: a general Monte-Carlo classical trajectory computer program. QCPE No. 453. An updated version of this code is VENUS96. Hase, W. L.; Duchovic, R. J.; Hu, X.; Komornik, A.; Lim, K. F.; Lu, D.-H.; Peslherbe, G. H.; Swamy, K. N.; van de Linde, S. R.; Varandas, A. J. C.; Wang, H.; Wolf, R. J. VENUS96 *QCPE Bull*. **1996**, *16*, 43.
(31) Marques, J. M. C.; Wang, W.; Pais, A. A. C. C.; Varandas, A. J. C. *J. Phys. Chem*. **1996**, *100*, 17513.
(32) Rodrigues, S. P. J.; Varandas, A. J. C. *J. Phys. Chem. A* **1999**, *103*, 6366.
(33) Davies, M. J. *J. Chem. Phys.* **1985**, *83*, 1016.
(34) Hutchinson, J. S.; Reinhardt, W. P.; Hynes, J. T. *J. Chem. Phys.* **1983**, *79*, 4247.
(35) Müller, R. P.; Hutchinson, J. S.; Holme, T. A. *J. Chem. Phys*. **1989**, *90*, 4582.